

1 Sudden acceleration of flames in open channels driven by hydraulic resistance

2 J. Yanez^{1*}, M. Kuznetsov¹, V. Bykov¹

3
4 ¹ Karlsruhe Institute of Technology, 76131 Karlsruhe, Germany

5
6 *Corresponding author: jorge.yanez@kit.edu

7
8 Hydrogen-air deflagrations with venting at the end of obstructed tubes are studied experimentally
9 and numerically. A *shockless* transition to the so-called *choked regime* of the flame propagation
10 is reported. Mixtures with 13% vol. of hydrogen were ignited from the open end of the tube at
11 the interface between fuel and the ambient air. Three venting ratios were selected, closed, 40%
12 and 100%. In all cases the flame initially propagates without acceleration at a velocity close to
13 the laminar flame speed. The flame configuration excludes most of conventionally
14 acknowledged phenomena of the DDT, namely, volumetric explosions, igniting shock and shock
15 waves interactions. However, after an induction period, of the order of 1 sec, the flame
16 accelerates more than 100 times, within a period of 3-30 ms, until the steady-state *choked* regime
17 is established. The mechanism of such rapid acceleration is investigated both numerically and
18 analytically. A one dimensional reduced description was suggested and analyzed to model the
19 process of the flame acceleration. The study of the over simplified model reveals that the
20 hydrodynamic resistance of the tube causes sudden flame acceleration and governs initial stage
21 of the DDT.

22
23 **Keywords:** DDT, turbulent flames, pressure driven flames, flame acceleration.

24 **1. Introduction**

25 Deflagration experiments in tubes are usually initiated by a weak source of energy, like a spark,
26 which produces the ignition of the reactive mixture in one of the extremes of the channel. The
27 flame propagates slowly in the beginning with a velocity that depends on the mixture reactivity
28 and may vary between several centimeters and several meters per second. The presence of
29 obstacles in a confined media affects the deflagration. The local expansion of the burned gases in
30 close proximity to obstacles generates turbulence that in a feedback mechanism increases the
31 effective burning rate causing an acceleration of the propagation of the flame. This cycle drives
32 the flame acceleration leading to high pressures within the reaction zone and, under certain
33 circumstances, to transition to detonation. This transition is very sensitive to small perturbations,
34 for instance, for lower reactive mixtures this feedback loop may be countered, or even
35 interrupted, by the tendency of the flame to quench due to stretch and heat losses. Furthermore,
36 lateral or end venting would cause energy and momentum losses that may slow down the flame
37 and prevent detonations and sonic propagation regimes.

38

39 Most of the previous investigations dedicated to the acceleration of flames in obstructed channels
40 have devoted a special emphasis to the deflagration to detonation transition (DDT) e.g. Bradley
41 et al. (2008) and Oran and Gamezo (2007). The problem of the transition from deflagration to
42 detonation regimes of the flame propagation was investigated in closed tubes (half closed),
43 where an ignition source was placed against the closed end.

44

45 Dorofeev et al. (2000 and 2001) and Kuznetsov et al. (2002) have developed some criteria to
46 predict the flame propagation regime in tubular configurations. Following those authors, the

47 expected regimes depend on the tube geometry, and specifically, on the configuration of the
48 obstacles. The stationary modes of the confined flame propagation can be classified as *slow sub-*
49 *sonic*, *sonic (choked)*, *fast super-sonic* and *quasi-detonations* (due to the considerable
50 momentum loss at the baffles the Chapman-Jouguet propagation velocity is not reached in
51 obstructed tubes).

52

53 *Fast* and *quasi-detonations* regimes may be suppressed by the use of venting orifices. Ciccarelli
54 et al. (1998) and Alekseev et al. (2001) experimentally investigated the effect of the lateral
55 venting on flame acceleration and DDT. It was found that the amount of reactive mixture
56 necessary for the development of sonic flames or DDT grows with an enlargement of the venting
57 surface. A comparison between end- and side-vented explosions in tubes showed a higher
58 efficiency of the end opening reducing the combustion pressure (Alexiou and Andrews 1997).

59

60 Although the most important stationary regimes (deflagration, fast subsonic, sonic and
61 supersonic, choking, quasi- and detonation regimes) their multiplicity and peculiarities have
62 been studied extensively and understood quite well (see e.g. Brailovsky and Sivashinsky (2000))
63 the transition between these combustion modes is still poorly understood and it represents very
64 complex open problem.

65

66 In the current study flames propagating in obstructed channels ignited from its open end are
67 investigated. The initial stage of the DDT – initial transition of the deflagration to fast subsonic
68 flames is in the focus of the study. In such configuration, a prolonged *quasi-laminar* propagation

69 phase is followed by a sudden and extremely violent *shockless* flame acceleration that culminates
70 when the *sonic* regime is reached.

71
72 Actually, the main mechanism of this sudden acceleration of flames was suggested by
73 Brailovsky and Sivashinsky (2000). However, in their studies the main focus was made on the
74 transition of the fast sub/super-sonic flames to the detonation and on multiplicity of the
75 detonation regimes themselves (quasi-detonation, fast flames driven by the diffusion of the
76 pressure etc.). The conclusion obtained from their numerical analysis was that the ultimate cause
77 triggering the DDT was the hydraulic resistance. In subsequent analytical and numerical studies
78 (see e.g. Bykov et al. (2004), Sivashinsky (2007)) the role of the hydraulic resistance was further
79 investigated and it was realized how markedly resistance affects the evolving flame.

80
81 The previous existing study dedicated to this non-typical flame acceleration behavior (see the
82 simulations performed by Middha and Hansen (2008)), confirms the sudden transition, but it
83 does not focus on driving critical mechanisms and does not include an analysis of the underlying
84 physics.

85
86 It is clear that the existence of friction forces destroys the *quasi-laminar* deflagration wave as a
87 stationary travelling wave. Nevertheless, the critical parameters driving this phenomenon and the
88 form in which this destruction occurs remains unclear. In order to improve current understanding
89 of the phenomenon, the authors have carried out the analysis presented in this article by
90 combining experimental, numerical and analytical approaches to the problem.

91 **Figure 1.**

92 **2. Description of the experiments**

93 The experiments were performed in the DRIVER facility (Scholtyssek et al., 2000), which is an
94 obstructed combustion tube with a total length of 12.2 m and an internal diameter of 174 mm,
95 (see Figure 1). The degree of obstruction selected was equal to 0.6. A 13% vol. hydrogen-air
96 mixture at ambient conditions was ignited at the open end, directly at the interface between the
97 inflammable mixture and the surrounding air. The instrumentation included photo diodes and
98 pressure gauges installed along the channel. The venting ratio α of the orifice was varied from
99 0% (fully closed) up to 100% (fully open).

100 **Figure 2**

101 In Figure 2 the experimental distance-time (x-t) diagrams of the flame propagation for closed
102 (left) and vented channel (right) are shown, representing pressure and light records plotted
103 against time in vertical direction. In the closed channel (left), the flame accelerates immediately
104 after reaching the first obstacle generating an additional flow motion which steepens into the
105 shock wave. The turbulent flow ahead of the flame created by the thermal expansion of the
106 products supports the flame acceleration within a relatively short time after ignition (~ 0.1 s).
107 Beyond the run-up distance, of about 1.3 m, the flame reaches the *choked* regime and propagates
108 further with a steady velocity of 540 m/s (close to the sound velocity in the product) and with the
109 characteristic pressure of the leading shock wave oscillates from 6 to 11 bar.

110 In the presence of venting, combustion products are discharged in the atmosphere through the
111 end orifice (Fig. 2, right) and do not support flame acceleration. The flame propagates in a *quasi-*
112 *laminar* regime with a stationary velocity of 3.5 m/s. The experimental records show that during
113 this phase no significant pressure increments exist (≈ 300 Pa) and, therefore, no relevant flow
114 motion (generating turbulence) appears ahead of the flame. Nevertheless, around 1 s after the

115 ignition, the flame suddenly accelerates from the *quasi-laminar* to the *choked* regime within the
116 same interval of 3-30 ms. After the acceleration, the *choked* flame propagates until the end of
117 tube with a constant velocity of 540 m/s creating peaks of pressure of 5-9 bar.

118 Experiments performed with different vent ratios showed that the run-up-distance, necessary to
119 reach the sonic propagation, is proportional to the vent ratio. They established that even a fully
120 open end cannot prevent flame acceleration to the sonic regime and demonstrate that the
121 acceleration mechanism may trigger a DDT in vented tubes of larger diameters with more
122 reactive mixtures.

123

124 **3. Numerical simulation**

125 Numerical simulations of the experiments were carried out with the combustion code *COM3D*
126 (Kotchourko, et al. 1999) developed in the Karlsruhe Institute of Technology. In order to analyze
127 the mechanism of the flame acceleration in presence of end discharge three values of the venting
128 ratio were selected, 0%, 40% and 100%.

129

130 **3.1. Modelling**

131 The numerical representation of the problem include the geometry of the tube, the obstacles
132 inside it and a supplementary volume with *open-non reflective* boundary conditions to simulate
133 the release of the combustion products through the vent area into the atmosphere. The *open-non*
134 *reflective* boundary conditions numerically reproduce the unconfined ambient air. The total
135 volume and time to be simulated restrict the minimum resolution achievable to 5.8 mm due to
136 the available computational power. Thus the Kolmogorov and Taylor turbulent micro-scales
137 remain smaller than the grid size. Likewise, the integral scale of the turbulence is minor than the
138 grid resolution. Moreover, the boundary layers remain largely unresolved making the use of wall

139 functions necessary. Furthermore, the laminar flame thickness is going to be lesser than the grid
140 size.

141 To overcome those restrictions, the KYLCOM combustion model (Yanez, 2010), specifically
142 designed for *under-resolved* calculations, and the standard k-ε turbulence model (Launder and
143 Sharma 1974) was utilized (restrictions of k-ε turbulence model appear i.e. Pope 2000). The
144 resolution adopted prevented the use of *Large Eddy Simulation* methods for the turbulence
145 modeling (for resolution requirements refer to (Jimenez 2004)). The initial levels of turbulence
146 and dissipation were chosen following the criteria of Arntzen (1998) making k and ε equal to
147 $1 \cdot 10^{-4} \text{ m}^2/\text{s}^2$ and m^2/s^3 respectively. For the modeling of the combustion the *KYLCOM* model
148 (Yanez, 2010) was coupled with the turbulent burning velocity correlation proposed by Schmidt
149 et al. (1998).

150 The influence of the resolution in the flame and hydrodynamic instabilities requires further
151 considerations. Until the flame acceleration takes place, the *thermo-diffusive* instability plays an
152 important role (see Figure 3, left), as confirmed by the experimental data of Kuznetsov et al.
153 (1998) and the analysis Zeldovich et al. (1988).

154 **Figure 3**

155 Contrary to the case of closed tubes where wrinkling is meaningful only until the first obstacle is
156 reached, in tubes with venting, the *quasi-laminar* propagation region grows significantly and the
157 effect of flame folding becomes very important. Thus, to estimate the increase in burning
158 velocity due to this, the following relation due to Driscoll,

$$159 \quad \Xi = \frac{1}{Le} \tag{1}$$

160 was utilized, where Ξ is the increase in burning velocity due to thermal-diffusive effects and Le
161 is the Lewis number of the mixture.

162 The *Kelvin-Helmholtz* instability is only partially resolved in the selected mesh. It may appear
163 (Kuznetsov, 1998) due to the interaction of the flame with obstacles (see Figure 3 right) but only
164 after the acceleration of the flame has started already. Therefore no special modeling was
165 considered for this effect.

166 **4. Results and analysis**

168 **4.1. General discussion**

169 Figure 4 displays a comparison of the flame propagation obtained from the results of simulations
170 and experiments. The results obtained for the *closed* case shows the characteristic fast
171 acceleration typical of those problems. For the cases with venting, two regions with different
172 propagation regimes, *fast* and *slow*, can be clearly identified.

173 **Figure 4**

174 The repeatability of the essays was analyzed repeating the test with 40% of venting twice. The
175 results of the two experiments show significant divergence of the transition location confirming
176 high sensitivity of the transition to the initial conditions and systems parameters. However, the
177 order of magnitude of the transition time and location as well as all properties of the transition
178 (initial deflagration velocity, thickness of the sharp acceleration region etc.) remains akin. The
179 second test for 40% of venting and the experiment with 100% venting almost superpose and the
180 acceleration of the process suffers a 40% delay (from ~ 0.6 s to ~ 1.0 s after the ignition). The
181 results of the numerical simulation for 40% of venting appear in the interval between the two
182 experimental curves and therefore a positive agreement between both can be claimed.

183 In the test performed with 100% of venting a significant delay in the transition to the *fast* flame
184 regime appear in the numerical calculations. The repeatability of the 100% venting case was not
185 analyzed experimentally, and therefore the time range uncertainty for the acceleration can be
186 estimated, by comparison with the 40% case, as the time registered in the experiment $\pm 40\%$.

187 The time necessary for the change of combustion regime is another representative magnitude of
188 the problem. Its value was approximately 50 ms in the calculations, while in the experiments the
189 intervals between the gauges restrict the accuracy of the measurements to a range of 3-30 ms.

190 Although the authors admit the need in further detail studies to comprehend the discrepancies
191 between different experiments it is considered as one of the characteristic inherent to this type of
192 combustion problems.

193 In the *choked* propagation area (almost vertical sections), the results of the experiments and the
194 calculations agree rather well. The simulation of the closed case was already the object of a
195 previous investigation (Yanez et al. 2010). Therefore, further details about it are not included
196 here.

197

198 **4.2. Borghi diagram analysis**

199 A preliminary insight into the occurring acceleration processes can be obtained with the help of
200 the Borghi diagram (Borghi, 1988). For the systematic mixture examination, the Karlovitz,
201 Damköhler, Lewis and Markstein numbers were calculated (see Table 1). The *Karlovitz* number,
202 was defined (Poinsot, 1991) as $Ka = u' / S_1 \sqrt{v / u' L}$, the *Damköhler* number as

203 $Da = S_L^2 L / (\chi u')$, the *Lewis* number as $Le = \chi / D$, and the *Markstein* number (Zeldovich

204 1985), as $Ma = \frac{\chi - D}{\chi} \frac{E_a (T_b - T)}{2RT_b^2} + \frac{D}{\chi}$.

205 **Table 1.**

206 All magnitudes necessary to perform the analysis were obtained in the same location, slightly
207 ahead of the flame front. This location corresponds, for the *closed* and *vented* cases, to
208 acceleration and quasi-laminar propagation regime respectively. In the case of the *choked*
209 propagation, the data was sampled between the initial shock and the sonic flame.

210 **Figure 5**

211 Figure 5 shows two differentiated combustion regimes. In the *closed* case, a regular accelerating
212 flame is found (black diamond). The *quasi-laminar* propagations obtained for the cases with
213 venting (white symbols) are deeply inside the *laminar flame* region. During the flame
214 acceleration, the white dots will describe a vertical path, moving out of the *laminar* region,
215 traversing an area near the black diamond to finalize in the position of the *cross* symbol which
216 represents the *choked* regime. The location of the *cross*, inside the *thickened flames* region,
217 indicates that the flame is quite stable and confirms its capability to accelerate to the *sonic*
218 propagation regime. In a very short time, a flame propagation regime in which no interaction
219 with turbulence existed is substituted abruptly by a saturated turbulence interaction.

220

221 **4.3. Analysis of the acceleration mechanism**

222 While the flame penetrates in the tube, the combustion products are discharged into the
223 atmosphere via the venting orifice. The propagation of the flame inside the channel implies that
224 combustion products should traverse a longer distance until they are discharged suffering an

225 enhanced *momentum loss*. The hydrodynamic resistance may be expressed through the formula,
226 Brailovsky and Sivashinsky (2000)

$$227 \quad F = -\frac{2c_D}{d} \rho u^2 \quad (2)$$

228 in which c_D is the drag force coefficient. The results of the numerical experiments carried out
229 with diverse flow velocities in the range 1-30 m/s allow approximating c_D with the value 0.12.
230 Therefore the total *loss of momentum* can be estimated as

$$231 \quad \Delta P = \int_0^{x_f} F dx$$

232 where integration is taken until the flame front position. The existence of obstacles increases the
233 complexity in the flow pattern. For the propagation of the flame in the laminar regime the
234 obstacles produce a change in the total surface of the flame and thus of the total fuel
235 consumption. In first approach this change can be estimated to be of the order of (1-BR) being
236 BR the Blockage Ratio. As the obstructions are gradually reached, cyclic oscillations in the
237 pressure (order of tens of Pa, peak of ~340 Pa, see Figure 6) as well as in the velocity of the
238 discharge products (see Figure 7) will appear. Those oscillations will have a frequency
239 $\omega_1 = \dot{x}_f / d$ where \dot{x}_f is the velocity of the flame front and d is the interval between obstacles,
240 which in this problem is equal to the diameter. Nevertheless, it is important to underline that no
241 shock waves develop during the entire quasi-laminar regime.

242 **Figure 6**

243 Figure 6 shows how pressure variations slightly compress and decompress the part of the tube
244 filled by the reactants. This area can be understood as a close cylinder, or a *drum*, in which the
245 flame actuates as an oscillating piston. In order to study the compression/decompression cycle of

246 the reactants the one dimensional Euler's equations of continuity and impulse may be used to
247 model the phenomenon. Performing cross derivatives on them (in t-x) and operating, the wave
248 equation can be obtained supposing the velocity of the oscillations is small and thus the
249 hydrodynamic resistance can be neglected. Additionally, by taking into account the observations
250 performed during the numerical experiments, the oscillations inside the reactants resulted to be
251 mainly of the first harmonic. The wave equation may thus be simplified to

$$252 \quad \ddot{p} + \left(\frac{2\pi c}{4(L-x_f)} \right)^2 p = 0 \quad (3)$$

253 where L is the total size of the tube, c is the local sound velocity in the fresh mixture and x_f is the
254 position of the flame, and therefore a second cyclic process with a frequency

$$255 \quad \omega_2 = \frac{c}{4(L-x_f)} \quad (4)$$

256 is present in our system, as can be seen in Figure 6 and Figure 7.

257 **Figure 7**

258 The final pressure signal obtained, are the superposition of the two cyclic processes with
259 frequencies ω_1 and ω_2 , and the variable peaks of the registered amplitudes results from this
260 superposition.

261 The resistance of the products grows linearly as the flame penetrates inside the tube (see Figure
262 6, thick line (trend)). When the resistance is comparable with the pressure peaks created by the
263 flame, the products have difficulties to be discharged and a part of them are accumulated inside
264 the tube. The reactants receive an enhanced compression and thus an increased compression-
265 decompression cycle is triggered. The flame suffers an additional acceleration and traverses an
266 augmented distance per oscillation. Some significant flow appears ahead of the flame. If during

267 this displacement an obstacle is overcome, the burning rate will be enlarged by the turbulence
268 created by the barrier and the flame starts to burn in the turbulent regime. The burning rate, the
269 compression of the reactants and the hydrodynamic resistance are thus enhanced.

270 **Figure 8**

271 Next compression-decompression cycle (see Figure 8, left), will drive the flame to a very intense
272 acceleration that will ultimately finish in the *choked* regime. Figure 8 (right) shows the behaviour
273 of experimental light and pressure signals in the nearest proximity to the sonic flame transition
274 point. At this position, the pressure oscillations due to the tube resistance become relatively
275 strong initiating the mentioned mechanism.

276 Clearly, a smaller vent surface will reduce the run-up distance due to the enhanced *loss of*
277 *momentum* on the orifice itself. Therefore, the critical value necessary to create overpressure and
278 flow ahead of the flame will be achieved faster.

279 The coupling between the described phenomena is very complex. The small, but predictable,
280 discrepancies between the repeated experiments with 40% of venting (Figure 4) caused by the
281 distinct timing of the flame acceleration (i.e. the flame traverse the same length but only one
282 obstacle is trespassed).

283

284 **4.4. One dimensional reduced model**

285 The discussion above hints on the possibility to use a one dimensional model of the propagation
286 of the flame. In the following a coarse tube is considered to simplify the model and make it
287 treatable analytically, in which the effect of the obstacles is taken into account as an enhanced
288 hydrodynamic resistance. Two separate regions of the tube are considered for the modeling. In
289 the so-called products region, between the flame and the discharge orifice the flow is assumed to

290 be incompressible. For the reactants, region between the flame and the closed end of the tube,
 291 the velocity is considered to be small and the term $u \cdot (\text{grad } u)$ can therefore be neglected during
 292 the initial flame acceleration stage.

293 Thus, the equation of the momentum conservation

$$294 \quad \frac{\partial \rho u}{\partial t} + \frac{\partial \rho u^2}{\partial x} + \frac{\partial p}{\partial x} = F. \quad (5)$$

295 for the region of the products, between the flame and the discharge orifice, becomes

$$296 \quad \rho \frac{\partial u}{\partial t} + \frac{\partial p}{\partial x} = F. \quad (6)$$

297 Taking into account the open end and typical deflagration velocities before the flame
 298 acceleration, incompressible flow in the products region is assumed as well. In the case of
 299 propagation of the flame in the deflagration laminar regime, and considering the reactants as
 300 incompressible, the velocity of the products can be defined as

$$301 \quad u = -(\sigma - 1)\dot{x}_f, \quad (7)$$

302 with σ expansion ratio, which follows from the mass conservation and from the mean flame
 303 surface velocity. Substituting (2) in (6) and integrating between the open end of the tube and the
 304 position of the flame yields

$$305 \quad -\rho \int_0^{x_f} (\sigma - 1)\ddot{x}_f dx + \int_0^{x_f} \frac{\partial p}{\partial x} dx = \int_0^{x_f} F dx \Rightarrow -\rho(\sigma - 1)\dot{x}_f x_f + p_f - p_0 = \int_0^{x_f} F dx. \quad (8)$$

306 Substituting (2) in (8)

$$307 \quad -\rho(\sigma - 1)x_f \ddot{x}_f + p_f - p_0 = -\frac{2c_D}{d} \rho(\sigma - 1)^2 \dot{x}_f^2 x_f \quad (9)$$

308 This equation contains p_f , pressure in the products side, as a free parameter that can be closed
 309 with the equation (3) obtained for the pressure in the reactants area. The increment of pressure

310 between both sides, in the case of a stationary flame front can be calculated applying Rankine-
 311 Hugoniot conditions

$$312 \quad \Delta p \approx \rho \sigma (\sigma - 1) \dot{x}_f^2 \quad (10)$$

313 **Figure 9**

314 With the help of this equation, the pressure in the reactants, p_f^+ side can be considered

$$315 \quad \rho(\sigma - 1)x_f \ddot{x}_f - p_f^+ + \rho\sigma(\sigma - 1)\dot{x}_f^2 + p_0 = \frac{2c_D}{d} \rho(\sigma - 1)^2 \dot{x}_f^2 x_f \quad (11)$$

316 This equation can be re-written considering the over-pressure, P . If $\dot{x}_f(0) = S_L$ then the over-
 317 pressure can be written as $P = p_f^+ - \rho\sigma(\sigma - 1)S_L^2 - p_0$

$$318 \quad \rho(\sigma - 1)x_f \ddot{x}_f = P - \rho\sigma(\sigma - 1)(\dot{x}_f^2 - S_L^2) + \frac{2c_D}{d} \rho(\sigma - 1)^2 \dot{x}_f^2 x_f \quad (12)$$

319 so that initially for $t=0$, $P(0)=0$.

320 This equation can be coupled with the equation (3) transformed for the over-pressure, which is

$$321 \quad \ddot{P} + \left(\frac{2\pi c}{4(L - x_f)} \right)^2 P = 0, \quad (13)$$

322 to obtain a closed system. The result of this problem, considering as initial conditions $t=0$,
 323 $x_f(0)=0.1$, when walls are reached by the flame with velocity $\dot{x}_f(0) = S_L$ are shown in Fig. 9. The
 324 initial conditions for the pressure were obtained from the numerical experiments and where
 325 $P(0)=0$ and $\dot{P}(0) = 10$. Although there is a good agreement of the results obtained with the one
 326 dimensional simplification it has to be underlined that the validity of the analysis is restricted to
 327 the initiation stage of the acceleration of the flame. Moreover, significant divergences obtained
 328 in the reproduction of experiments themselves and of numeric simulations (compare critical

329 times shown in Figs. 4 and 9) may then be mathematically expressed through strong dependence
 330 of the early flame development.

331 In order to illustrate this and explain the core mechanism of the flame acceleration let us consider
 332 the equation (12) without the overpressure term, namely, $P(t)=0$ is assumed.

333 **Figure 10**

334 The system has the final form

$$335 \begin{cases} \ddot{x}_f x_f = -\sigma((\dot{x}_f)^2 - S_L^2) + \frac{2c_D(\sigma-1)}{d}(\dot{x}_f)^2 x_f \\ \dot{x}_f(0) = S_L \\ x_f(0) = x_f^0 = 0.1 \end{cases} \quad (14)$$

336 This system is studied in the phase plane by transforming the ODEs equation of second order to
 337 a plane system of ODEs of the first order via regular transformation:

$$338 \begin{cases} v = \dot{x} \\ u = \dot{v} \end{cases} \Rightarrow \begin{cases} \dot{v} = u \\ \dot{u} v = -\sigma(u - S_L^2) + \frac{2c_D(\sigma-1)}{d}u^2 v \end{cases} \quad (15)$$

339 The solution of the system in the phase plane coordinates looks

$$340 u = S_L \left(1 + \frac{4C_D(\sigma-1)}{d} \int_{x_f^0}^v s^{2\sigma} e^{-\frac{4C_D(\sigma-1)s}{d}} ds v^{-2\sigma} e^{\frac{4C_D(\sigma-1)v}{d}} \right)^{1/2} \quad (16)$$

341 Figure 10 shows the solution by the black dashed line. First observation concerns the limiting
 342 behavior of the system solution in the vicinity of zero

$$343 \int_{x_f^0 \rightarrow 0}^v s^{2\sigma} ds v^{-2\sigma} \approx \frac{v}{2\sigma} \rightarrow 0 \quad (17)$$

344 demonstrates that $x_f^0 \rightarrow 0$ can be justified and no singularity occurs at the initial point. The second
 345 and most important observation about the system initial behavior, namely, the role of the system
 346 isocline of the flame speed equation:

$$347 \quad \dot{u} = \left(-\sigma(u - S_L^2) + \frac{2c_D(\sigma - 1)}{d} u^2 v \right) / v = 0 \Leftrightarrow u^2 = \frac{d\sigma}{2c_D(\sigma - 1)} \left(\frac{S_L^2}{\frac{d\sigma}{2c_D(\sigma - 1)} - v} \right) \quad (18)$$

348 Figure 10 shows by the solid black line that near the origin it represents a stable attractor, all
 349 trajectories starting nearby converges (fast) to the lower branch of the isocline and follow the
 350 detailed solution. Moreover, right after crossing the isocline the system solution trajectories
 351 changes the character (speeding up instead of decreasing for initial point above the curve), this
 352 make the border line which is asymptotically given by

$$353 \quad v^* = x_f^* = \frac{d\sigma}{2c_D(\sigma - 1)} = 0.94 \quad (19)$$

354 a very important and crucial property defining the critical behavior. It explains the transition
 355 phenomena in terms of the phase plane. One clearly sees that if the initial point is on the right

356 from this curve $v = v^* = \frac{d\sigma}{2c_D(\sigma - 1)}$ the vector field demonstrates the exponential increase of the

357 flame speed as a function of the flame distance.

358
 359 Additionally, the form of the isocline dependence on the system parameters and variables

$$360 \quad u^2 = \frac{d\sigma}{2c_D(\sigma - 1)} \left(\frac{S_L^2}{\frac{d\sigma}{2c_D(\sigma - 1)} - v} \right) \quad (20)$$

361 predicts the sensitivity of the critical phenomena on the initial pressure perturbation with respect
362 to time, but the sensitivity is lower with respect to the space. Indeed, Fig. 10 (right) shows that
363 there is no so much difference in the space if one replaces $S_L^2 \rightarrow \alpha S_L^2$ in the equation.
364 Qualitatively, similar phase portrait is observed, with the same critical value for the space (flame
365 position) with the main speed up of the flame in between x_f^* and $2x_f^*$, while numerical values
366 of the critical time equal $t_f^*(\alpha = 1) = 1.241897$ and $t_f^*(\alpha = 0.75) = 1.430550$ respectively. A
367 weak sensitivity to the perturbation of the initial pressure and the form of the critical parameter
368 can be explained in more simple way. Namely, the found asymptotic of the equation physically
369 means that the flame starts rapidly accelerating whenever the pressure jump (drop of the pressure
370 - work of the pressure force) less or equals to the work of the friction forces.

$$371 \quad \Delta p = \rho \sigma (\sigma - 1) \dot{x}_f^2 \equiv \frac{2c_D \rho_- (\sigma - 1)^2}{d} (\dot{x}_f)^2 x_f^* = \int_0^{x_f^*} F(u(t, s)) ds \rightarrow x_f^* = \frac{d \sigma}{2c_D (\sigma - 1)} \quad (21)$$

372 Thus, when the work of the friction force starts dominate, the pressure in the reaction front
373 increases triggering the flame acceleration due to the cumulative effect of the pressure diffusion.

374
375 It is very important to note that there no regular singularity (reaching infinity in final time or
376 space as a reaction front position) was observed in the solution of the governing equations, just
377 very smooth and exponential (although hyper-geometric) growth of the system solution was
378 found to take place. This confirms, explains and fully justifies an irregular *shockless* character of
379 the flame acceleration observed in the experiments.

380

381 5. Conclusions

382 The problem of rapid acceleration of the flame in obstructed tubes with an open and vented end
383 was analyzed experimentally, numerically and analytically. In order to study the acceleration
384 problem of the flames propagating in tubes with different venting ratios the results of three
385 experiments were simulated numerically. The dynamics of the combustion process was
386 reproduced quite adequately by the numerical simulations. The obtained experimental results
387 show that the deflagration propagation regime instantly accelerates, without generating shock
388 waves, to the fast sonic flames inside a time interval of 3-30 ms. It was shown numerically that
389 this sharp flame acceleration is a consequence of the coupling between three effects: the pressure
390 oscillations of the closed space filled with reactants, the trespass of more than two obstacles by
391 the flame in a single oscillation phase and the hydrodynamic resistance that depends on the total
392 length passed by the products until they are discharged in the atmosphere. It was found that the
393 latter has a pivotal role and to the leading order it defines the actual critical transition length,
394 while the time of the transition is strongly influenced by the other factors. It has to be underlined
395 that the observed acceleration process involves a pure hydrodynamic mechanism, which was
396 confirmed by the analysis of one-dimensional simplified model. A parametric analysis performed
397 using the Borghi diagram demonstrates the possibility of such scenario of the flame propagation.
398 The same mechanism might be responsible for the detonation initiation in obstructed channels
399 with end venting in case of more reactive mixtures or larger tube diameter.

400

401 **References**

402 V. I. Alekseev, M. S. Kuznetsov, Yu. G. Yankin, S. B. Dorofeev, *Journal of Loss Prevention in*
403 *the Process Industries* 146 (2001) 591-596.

404

405 B. Arntzen, Modelling of turbulence and combustion for simulation of gas explosions in
406 complex geometries, Thesis for Dr. Ing Degree, The Norwegian university for science and
407 technology, (1998).

408

409 A. Alexiou, G.E. Andrews, H. Phylaktou, Process Safety and Environmental Protection 75 1
410 (1997) 9-13.

411

412 R. Borgi, Prog. Energy Combust. Sci. 14 (1988) 245-292.

413

414 D. Bradley, M. Lawes, Liu Kexin, Turbulent flame speeds in ducts and the
415 deflagration/detonation transition. Combustion and flame 154 (2008) 96-108.

416

417 I. Brailovsky, G.I. Sivashinsky, Combustion and flame 122 (2000) 492-499

418

419 V. Bykov, I. Goldfarb, V. Goldshtein, L. Kagan, G. Sivashinsky Combust. Theory Modelling, 8
420 (2004) 413-421

421

422 J. Chao, J.H.S. Lee, Shock Waves 12 (2003) 277.

423

424 G. Ciccarelli, J. Boccio, T. Ginsberg, C. Finfrock, L. Gerlach, H. Tagava, A. Malliakos, The
425 effect of lateral venting on deflagration-to-detonation transition in hydrogen–air steam mixtures
426 at various initial temperatures. NUREG/CR-6524, BNLNUREG-52518. Washington, DC: US
427 NRC, 1998.

428

429 S.B. Dorofeev, V.P. Sidorov, M.S. Kuznetsov, I.D. Matsukov, V.I. Alekseev, Shock Waves 10
430 (2000) 137-149.

431

432 S.B. Dorofeev, M.S. Kuznetsov, V.I. Alekseev, A.A. Efimenko, W. Breitung, Journal of loss
433 prevention in the process industries, 14 (2001) 583-589.

434

435 J.F. Driscoll, Prog. Energ. Combust. 34 (2008) 91-134.

436

437 J. Jimenez, Turbulence and Vortex Dynamics. Ecole polytechnique, Palaiseau, France, 2004.

438

439 A. Kotchourko, W. Breitung, A. Vesper, in: Deutsches Atomforum e.V. Annual Meeting on
440 Nuclear Technol, 1999.

441

442 M. Kuznetsov, V. Alekseev, Y. Yankin, S. Dorofeev, Combustion Science and Technology 174
443 (2002) 157-165.

444

445 M.S. Kuznetsov, I.D. Matsukov, V.I. Alekseev, S.B. Dorofeev. (1999) Photographic study of
446 unstable turbulent flames in obstructed channels. Proc. of the 17th ICDERS, 143.1-143.4

447

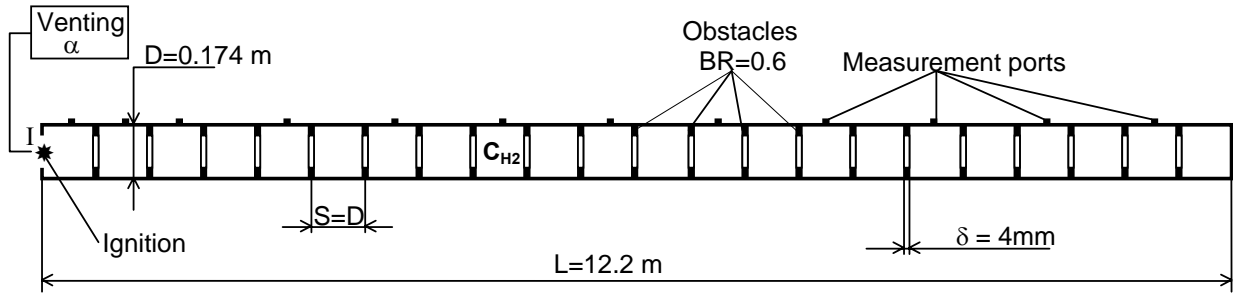
448 B.E. Launder, B.I. and Sharma, Lett. Heat Mass Trans 1(2) (1974) 131-138.

449

450 P. Middha, O.R. Hansen, Process Safety Progress 27(3) (2008) 192-204.

451
452 Oran, E.S.; Gamezo, V.N. *Combustion and Flame*, 148 (2007) 4-47.
453
454 T. Poinso, D. Veynante, S. Candel, *Journal of Fluid Mechanics*, 228 (1991) 561-606.
455
456 S.B. Pope *Turbulence flows*, Cambridge University Press, 2000.
457
458 H.P. Schmidt, P. Habisreuther, W. Leuckel, *Comb Flame* 113 (1998) 79-91.
459
460 W. Scholtyssek, A. Efimenko, M. Kuznetsov, Integral large scale experiments on hydrogen
461 combustion for severe accident code validation. FIKS-1999-00004, 344, 2000.
462
463 G.I. Sivashinsky, *Rev. R. Acad. Cien. Serie A Mat.*, 2001(2) (2007) 173-186.
464
465 J. Yanez, A. Kotchourko, A. Lelyakin, in: Bradley, D., Makhviladze, G., Molkov, V. (Eds.),
466 *Proceedings Sixth International Seminar on Fire and Explosions Hazards*, Research publishing,
467 2011, p. 137-149.
468
469 Ya. B. Zeldovich, G.I. Barenblatt, V.B. Librovich, G.M. Makhviladze, *The mathematical theory*
470 *of Combustion and Explosion*. Consultants Bureau, New York & London, 1985.
471

472



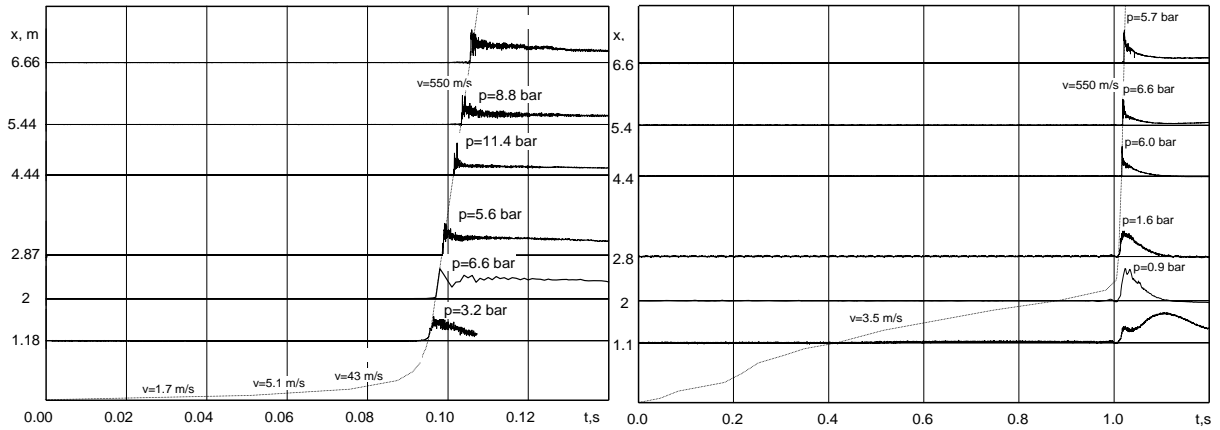
473

474

475

Figure 1: Combustion tube configuration

476



477

478

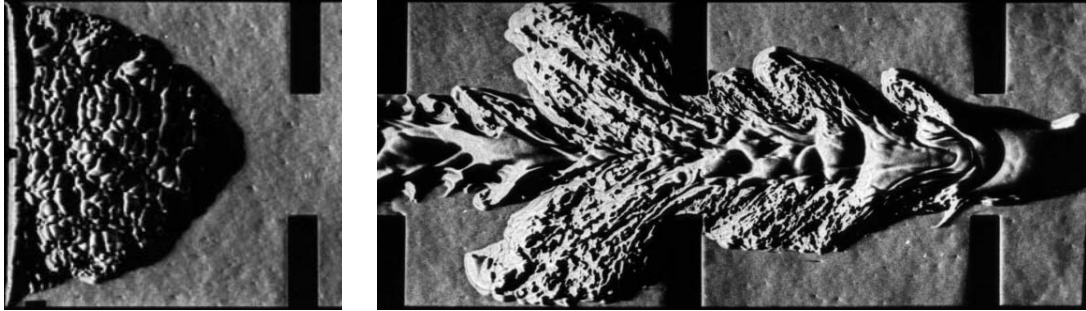
479

480

481

Figure 2: x-t – diagram of the initial flame propagation in closed (left) and 40%-vented (right) obstructed channels: flame front (FF) trajectory (blue dots); light signals (black lines); pressure records (red lines).

Pressure peaks and local visible flame velocities are shown at the plot.



482

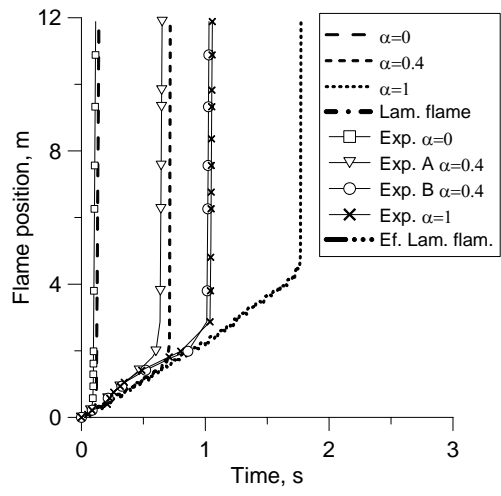
483

484 **Figure 3: Laminar flame front structure for tested mixture (13% H₂-air, Le=0.36, closed tube, ignition at the**

485

end flange) in case of thermo-diffusive (left) and Kelvin-Helmholtz (right) instabilities.

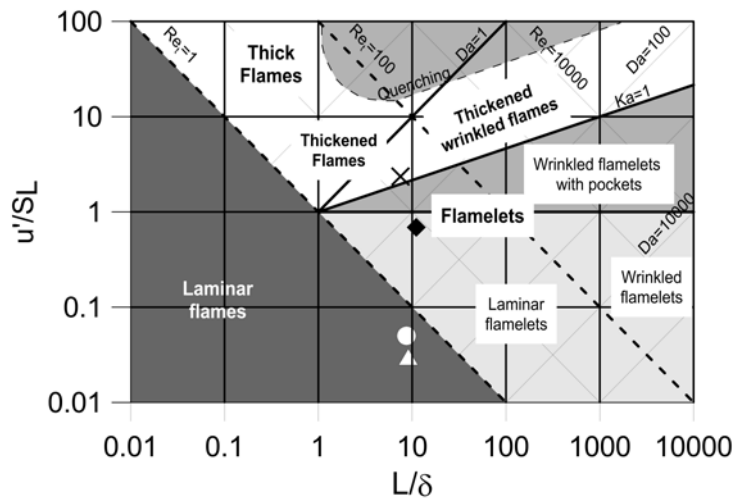
486



487

488 **Figure 4: Flame position. Dashed lines calculations. Thin continuous lines with symbols, experiments. Thick**
 489 **lines, laminar and quasi laminar regime propagation. Venting ratio is indicated in the legend.**

490

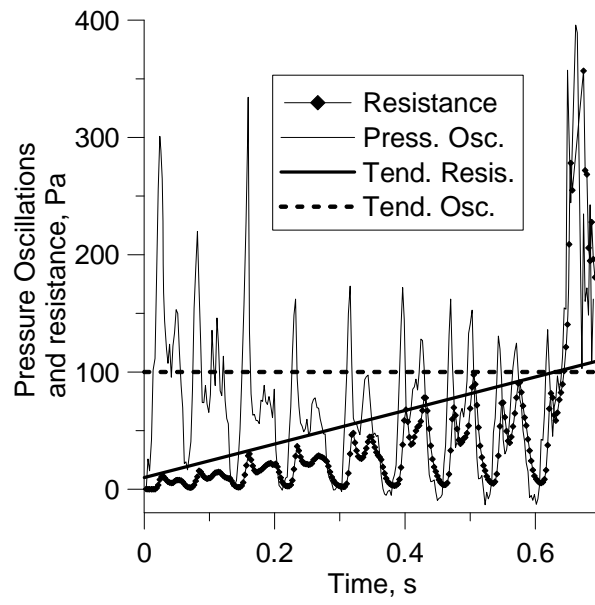


491

492

Figure 5: Borghi Diagram. Diamond $\alpha=0$, circle $\alpha=0.4$, triangle $\alpha=1$, cross *choked* regime.

493

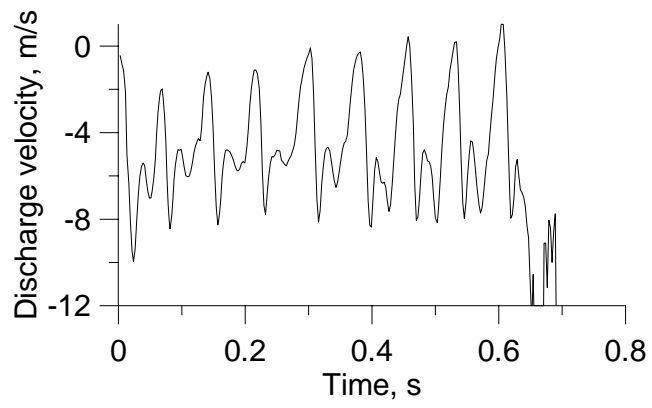


494

495

Figure 6: Pressure oscillations and resistance obtained for the case $\alpha=0.4$.

496

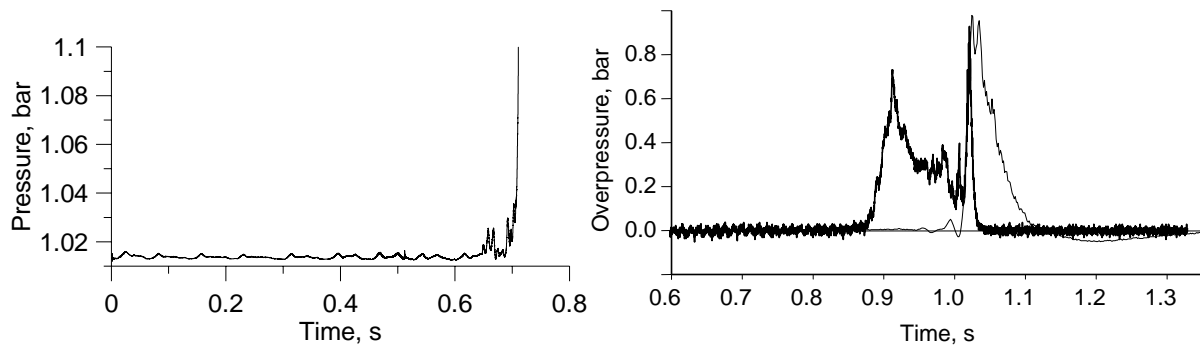


497

498

Figure 7: Discharge velocity in venting orifice for the case $\alpha=0.4$.

499



500

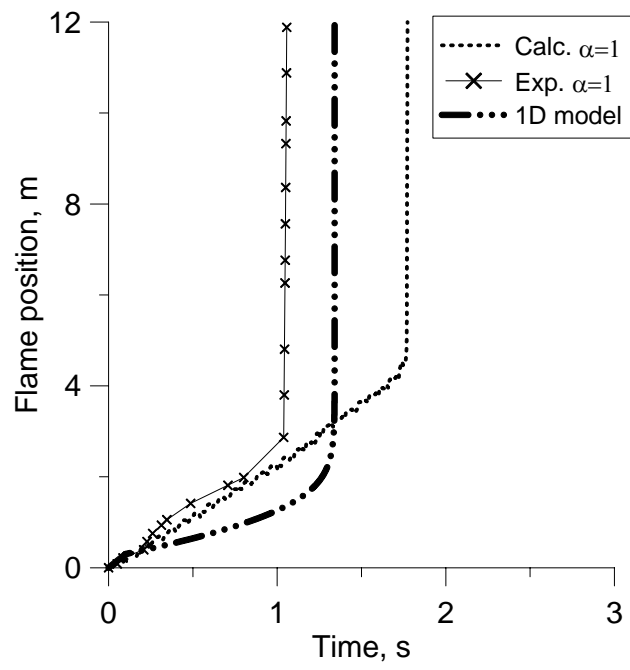
501 **Figure 8: Pressure records. Left, numerical simulation at the moment of the flame acceleration. Signal**

502 **clipped at 1.1 bar. Right, experimental. Light signal (thin), pressure signal (thick).**

503

504

505

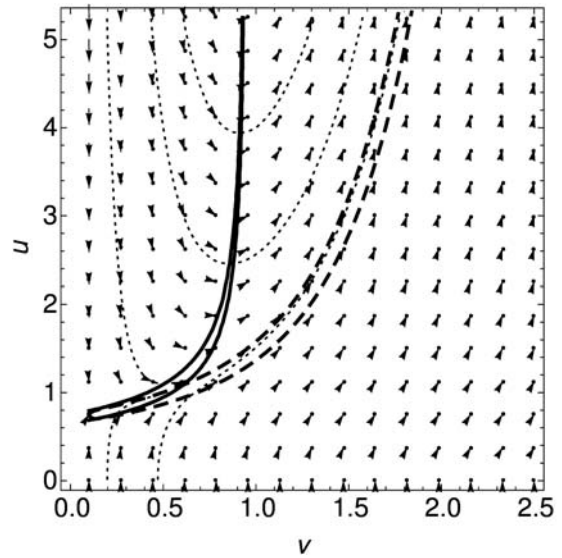
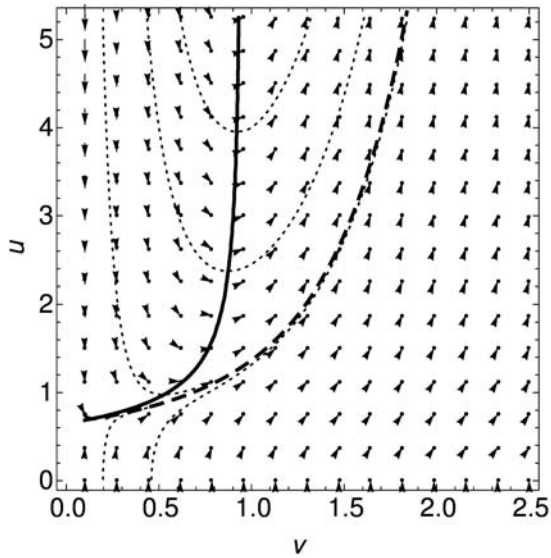


506

507

Figure 9: Flame position. Comparison of calculations experiments and one dimensional model.

508



509

510 **Figure 10:** Phase portrait $(x, \dot{x}) = (v, u)$ of the reduced model is shown with system solution trajectories
 511 and a vector field. Green line shows the isoclines of the reaction wave speed showing minimal possible flame
 512 velocity for a given initial state x . Red and blue lines are streamlines of the vector field. Dashed line is the
 513 solution trajectory of the system. On the right both original and perturbed systems phase portraits are shown
 514 for $\alpha = (1, 0.75)$ and $S_L^2 \rightarrow \alpha S_L^2$.

515

516

517

Table 1: Characteristics of the gases before flame arrival. Different degrees of venting and *choked* regime.

Venting	Ka	Da	Le	Ma	S_L (m/s)	σ	Combustion regime
0.0	1.92	15.9	0.36	1.13	0.23	3.38	Laminar flamelets
0.4	0.03	188	0.36	1.13	0.23	3.38	Laminar flames
1.0	0.01	327	0.36	1.13	0.23	3.38	Laminar flames
-	9.91	3.18	0.36	1.13	0.23	3.38	Choked flame

518